Major non-volatile intermediate products of photo-catalytic decomposition of ethylene

Siteng Tieng, Zixian Jia, Sana Labidi, Ana Paola Diaz-Gomez Trevino, Pierre Eloy, Eric M. Gaigneaux, Khay Chhor, Andreï Kanaev

Major non-volatile intermediate products of photo-catalytic decomposition of ethylene

Siteng Tieng [1], Zixian JIA[1#], Sana Labidi [1], Ana Paola Diaz-Gomez Trevino [1], Pierre Eloy [2], Eric Gaigneaux [2], Khay Chhor [1], Andrei Kanaev[1]

[1] *Laboratoire des Sciences des Procédés et des Matériaux, CNRS, Université Paris 13, Sorbonne Paris Cité, Villetaneuse, France*

[2] *Université Catholique de Louvain, Unité de catalyse er chimie des matériaux diverses,Louvain-la-Neuve, Belgium*

[#] Corresponding Author
E-mail Address: zixian.jia@lspm.cnrs.fr

Abstract

A complex kinetics of the photocatalytic decomposition of gaseous ethylene on nanoparticulate Fe(III) doped anatase TiO_2 was analyzed in a continuous-flow fixed-bed reactor. The analysis evidenced the production of non-volatile intermediate reaction products, which cover the photocatalyst surface and delay the time of attaining the stationary reactor performance. As a result, the reaction yield slowly increases during the long-lasted (~3 hours) intermediate stage. Based on Raman, FTIR and thermal post-treatment analyses, we assigned the major non-volatile reaction product to polymeric oxidized hydrocarbons: furan and furfural oligomers. A theoretical model is proposed explaining the observed kinetics.

Key words: Photocatalysis, process kinetics, Fe-doped TiO_2 nanoparticles, ethylene, non-volatile products, polyfuran, polyfurfural

I. Introduction

Photocatalysis in the gas phase has attracted much attention during recent years because of its wide potential for air purification. The most commonly used photocatalyst is titanium dioxide (TiO_2) known for its photocorrosion resistance and low cost. The photocatalytic activity of this material is due to the generation of the electron–hole pair under UV light illumination. However, the major problem that restraints its industrial implementation is related to low quantum yield of the photooxidation reactions [1]. Cationic and anionic doping of TiO_2 is one of the typical approaches to enhance photocatalytic efficiency under UV light illumination. Researchers have investigated the effects of transition metal such as iron [2–4], which is much cheaper than noble metal such as Ag [5] and Au [6] on reducing band gaps, decreasing electron and hole recombination rate, and using visible light.

The heterogeneous photocatalysis generally involves intermediate reaction products, which desorption and reactivity affect the overall process efficiency. Their knowledge is of particular importance for the process optimization and rigorous comparison of the material activities. Between different pollutants, ethylene is often considered as the model one because of its seemingly simple decomposition scheme involving few intermediate reaction products. In the same time, the ethylene abatement remains one of important environmental tasks. The photocatalytic oxidation of ethylene has been largely reported in literature [7–11]. Several studies have addressed intermediate products of the ethylene photodegradation. Bhattacharyya et al. [12] have observed formic acid as the main by-product, while Wang et al. [13] have reported on the formation of aldehydes and alcohols. Einaga and Teraoka [14] have analyzed the ethylene photooxidationon TiO_2 doped with platinum. In the absence of water vapor, absorption bands in the range of 1200-1800cm^{-1} have been observed and attributed to oxygenated compounds containing C-O, COO^- and C=O groups. The concentration of these intermediate species decreases with the irradiation time in presence of water vapors, leading to their complete mineralization into CO_2. Several studies [15–17] have reported on the formation of ethane C_2H_6, while oxygenated hydrocarbons CH_3CHO, CH_3COCH_3 and $CH_3COC_2H_5$ were present in a small quantity. In the same time, non-volatile reaction products, capable remaining on the catalyst surface

and affecting the process kinetics and reaction yield, have not been investigated in previous studies, probably because of their not easy detection.

Previously, we have reported on the effective ethylene decomposition using nanoparticulate TiO_2 coatings homogeneously doped with Fe(III) [18,19]. A net difference in the photocatalytic kinetics between the first and subsequent reactor runs has been observed on the initial process stage, which could be related to a participation of unknown reaction products. In the present communication we report on the kinetics analysis of gaseous ethylene photocatalytic decomposition on nanoparticulate Fe(III) doped anatase titania. We assign major non-volatile reaction products and provide a theoretical model explaining their influence on the reaction kinetics.

II. Experimental methods

2.1 Sample preparation

The Fe(III)-doped TiO_2 anatase photocatalyst with the optimal composition was used in this work because of its higher reaction efficiency compared with a pure titania. The preparation procedure has been described in our previous works [18,19]. In short, the material was obtained in the two-stage process including (1) fabrication, doping and immobilization on a glass support of titanium-oxo-alkoxy (TOA) nanoparticles, followed by (2) thermal treatment of the nanoparticulate coating. The doping of TOA nanoparticles with Fe^{3+} ions was achieved at the nucleation stage. The homogeneity of the coating doping has been evidenced in the previous studies. The colloids have been prepared using hydrolysis ratio H= 2.0, which corresponds to one of the stability domains of the TOA sol–gel process and enables metastable chemically active monodispersed nanoparticles of size 2R=5.2 nm. The concentration of iron in TiO_2 was fixed to 0.005 mol%, which corresponds to the best photocatalytic activity of the coating [19]. The reactive colloid has been set in a short contact with the supporting material, preliminary treated with 95 mol% sulfuric acid at 70 °C for 4 hours and washed in ultrasound bath. The beads with the deposited photocatalyst were heat treated at 500 °C for 4 hours to obtain anatase crystalline phase.

For the synthesis, analytical grade reagents and distilled water were used. Iron (III) acetylacetonate of 99.9% purity was supplied by Sigma–Aldrich. Titanium tetraisoproxide (TTIP) and 2-propanol with respectively 98% and 99.5% purity were purchased from Acros Organics.

2.2 Sample characterization

The Fe(III)-doped TiO_2 anatase photocatalyst preparation was previously reported by our group [18,19]. The characterization of catalyst was summarized in supporting information. From Fig. S1, it is observed that the surface with mean roughness of ~0.5 nm and composed of agglomerates formed by particles of average size ~6 ± 3 nm which was also evidenced by TEM image (Fig. S1). The XRD (Fig. S3) indicates that Fe(III)–TiO_2 powder well crystallizes in the anatase phase in the considered temperature range. Fig.S4 displays XPS spectra of the doped samples in two relevant energy ranges of 450-470eVand530-540eV. In agreement with studies of pure TiO_2,photoemission bands appearing at 464.5 ± 0.2 eV and 458.7 ± 0.2 eV can be attributed to Ti $2p^{1/2}$ and Ti $2p^{3/2}$ states of Ti^{4+} and the signal associated with singlet oxygen was also observed at 530.0 ± 0.4 eV with a shoulder at 531.5 ± 0.3 eV. Fig.S5 shows typical XPS spectrum of our Fe(III)-TiO_2 coatings in the energy range 700-745eV.Because of the low Fe concentration, two weak signals were observed at 709.9 eV and 723.5 eV as well as the satellites of a very low intensity.

2.3. Photocatalytic experiments

The experimental conditions are listed in Table 1.

Table 1: Experimental conditions of photocatalytic experiments

Gas mixture flow rate	90 ml/min
Reactor length	30 cm
Photocatalyst mass	6,6 mg
Ethylene concentration	34 ppm
Relative humidity R_H	13 %
Pollutant residence time in the reactor tube	1,4 s

The photocatalytic experiments were performed with a laboratory gas-phase continuous flow fixed-bed reactor depicted in Fig.1. In short, air gas flow containing pollutant and water vapour passes

through the reactor tube made of transparent glass in the UVA spectral region of $\lambda \geq 320$ nm. The reactor tube of 6 mm diameter is surrounded by six 8-W lamps emitting at 362 nm ($\Delta\lambda_{hwfm}$= 22 nm). Ethylene concentrations before (C_{in}) and after (C_{out}) the reactor tube were analysed by a gas chromatography device (Varian CP 3800) equipped with two injection loops allowing measurements in a continuous sampling mode. The temperature of the photocatalytic bed was continuously monitored. The pollutant conversion (or reactor yield) is calculated according to $\eta(\%)=100\cdot(1-C_{out}/C_{in})$.

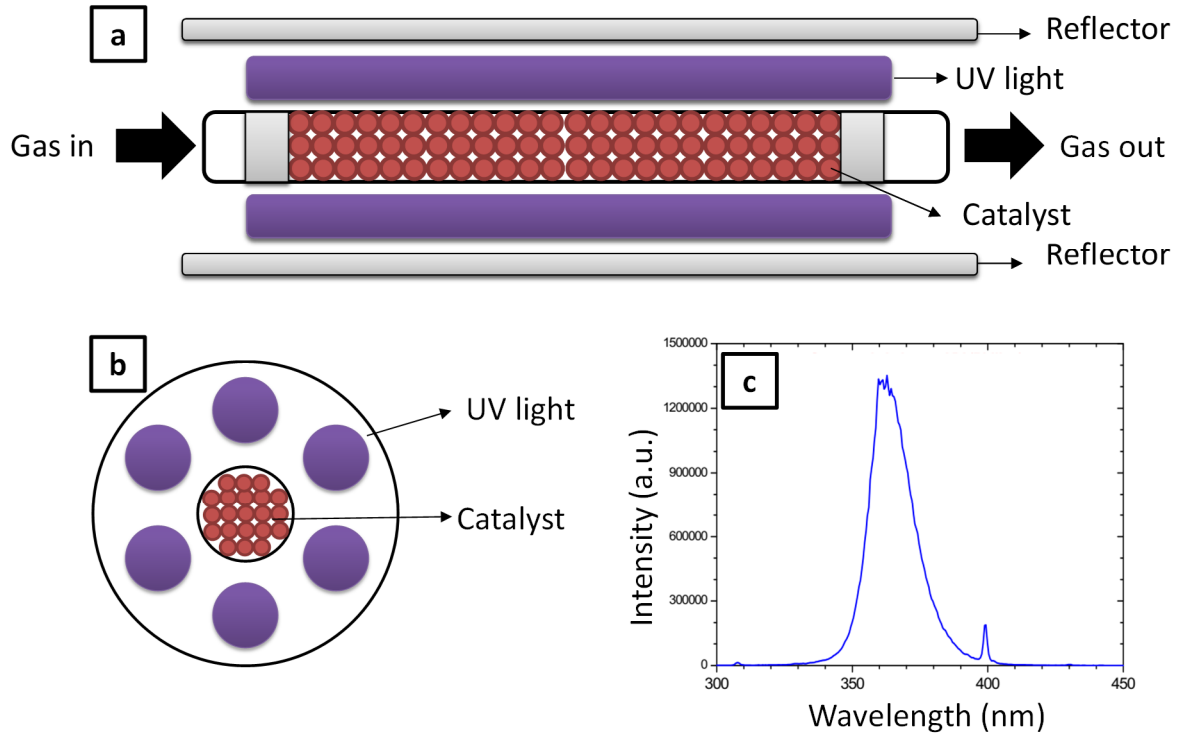

Figure 1. (a) Cut section and (b) cross section of the photocatalytic reactor and (c) Emission spectrum of the UV light.

III. Results and discussion

3.1 Intermediate reaction products

The ethylene conversion kinetics over the freshly prepared photocatalyst shows three main stages as depicted in Fig. 2a. (1) On the first stage $0 \leq t \leq t_1$ (t=0 corresponds to illumination of the reactor lamps), the ethylene conversion increases rapidly, which corresponds to the temperature increase (curve b in Fig. 2) that may thermally activate photocatalytic reactions. (2) The second stage taking

significantly long time $t_1 \leq t \leq t_2$ consists in a slow increase of the ethylene conversion, which is apparently controlled by the surface chemistry and reactive interface modification. (3) At the end of the second stage, the stationary regime is attained. This maximum stationary activity of the photocatalyst keeps over week without any signs of deactivation.

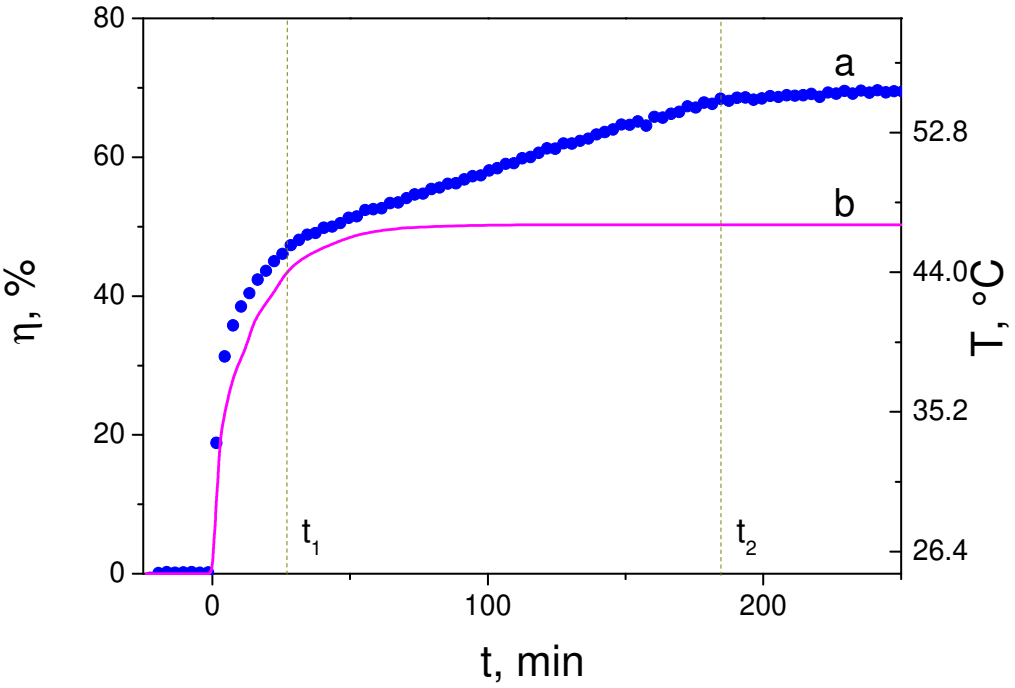

Figure 2. Ethylene conversion η (a) and temperature (b) of a fixed-bed continuous-flow photocatalytic reactor.

The slow intermediate stage 2 was only observed with the freshly prepared photocatalyst. This stage was absent with the reused material where the pollutant conversion rapidly attained the maximum level. The strong increase (almost twice) of the process efficiency during stage 2 suggests significant modification of the reactive interface that can be related to the accumulation of reaction products. Apparently, the known acetaldehyde [20] or CO_2-CO [21] cannot be candidates since do not accelerate the decomposition kinetics and may only slow it down by closing the active surface sites. In the same time, the gas chromatography analysis at the reactor exit did not evidence any significant traces of new products except for ethylene, CO/CO_2 and water. It is assumed therefore that the major kinetics modification at this stage is due to an unknown non-volatile product accumulated at the photocatalyst surface.

In order to confirm the presence of non-volatile intermediate products, accumulated during the transitory stage 2, photocatalyst already used in the process (which don't manifest the transitory stage and rapidly attains stationary performance) was exposed to a secondary thermal treatment. Such heat treatment under ambient air is expected to sublimate or burn the deposited species that converts the reactive interface to its original state. The photocatalytic test was performed after the secondary heat treatment in order to check if the reaction kinetics recovers. The results are shown in Fig. 3 the photocatalysts heat treated at temperatures (a) 60 °C for 3 hours under UV illumination (this reference series reproduces the reactor conditions), (b) 100 °C for 3 hours, (c) 200 °C for 3 hours and (d) 300 °C for 1 hour. One can see that the used photocatalysts exposed to temperatures $T \leq 200$ °C (Fig. 3a,b,c) do not regain the original kinetics, while that exposed to T=300 °C (Fig. 3d) restores kinetics of the freshly prepared material. These results indicate that the intermediates product involved in the photocatalytic process of ethylene decomposition has relatively high stability against desorption at the photocatalyst surface. Previous DSC-TGA measurements have evidenced the departure of the adsorbed alcohol and water at temperatures ~80 °C [22], which indicates that, the surface species are much heavier in our case. Consequently, it was suggested that the intermediate reaction products of the ethylene decomposition are strongly bound to the surface. Commonly, the temperature range 200 °C < T ≤ 300 °C corresponds to the burning of surface organics [23]. It is concluded therefore that photocatalytic decomposition of ethylene includes as an intermediate step the formation of stable non-volatile products at the photocatalyst surface.

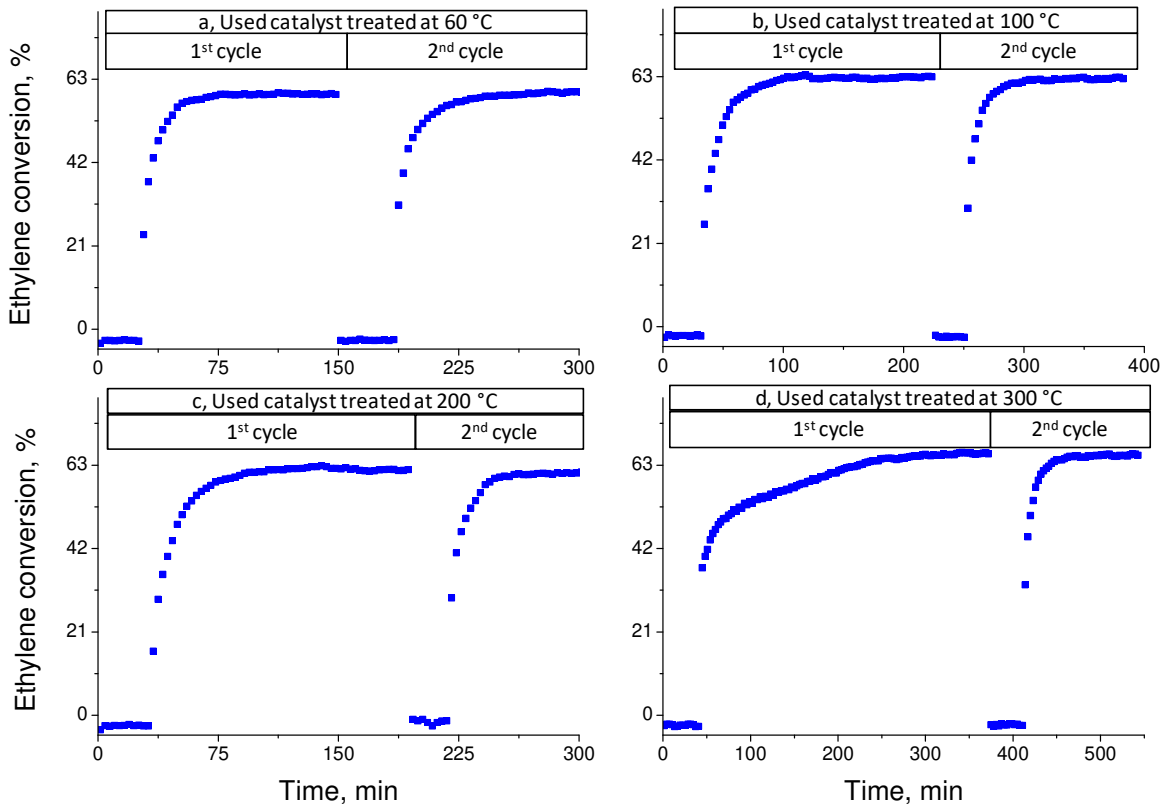

Figure 3. Ethylene conversion of used Fe(III)-TiO_2 photocatalyst subsequently heat treated in a dry air flow: (a) at 60°C during 3hours under UVA illumination, (b) at 100°C during 3 hours,(c) at 200°C during 3 hours and d) at 300°C during 1 hour. (Each photocatalyst has been studied in two repeated cycles).

In order to clarify the nature of these intermediate species, the FTIR analysis of the photocatalyst was performed after utilisation in the reactor. Fig. 4 displays IR spectra in frequency ranges of 1000-2000 cm^{-1} and 2400-4000 cm^{-1} of the freshly prepared catalyst (a) and that kept in the reactor under the pollutant flow during 10 hours with the UVA lamps off (b) and on (c). The presence of the adsorbed species at the catalyst surface was evidenced the appearance of absorption bands at 1070, 1150, 1360, 1480, and 2980 cm^{-1} in spectrum (c), in contrast to those of freshly prepared photocatalyst (a) and that exposed to the pollutant without UVA illumination (b) which look similar. Complimentary, FTIR spectra was measured with the used photocatalyst submitted to the secondary thermal treatment, as in the process kinetics measurements previously discussed in Fig. 3. The results are presented in Fig. 5. In agreement with the previous conclusion, the absorption bands of the adsorbed species at 1070, 1150, 1360, 1480, and 2980 cm^{-1} (a-b) begun to change after heating at 200 °C (c) and completely

disappear after being exposed to the temperature of 300 °C (d). This observation is consistent with the burning of organics chemically bound to the photocatalyst surface. The following assignment for the observed IR bands can be proposed. The large band around 3300 cm^{-1} belongs to O-H stretching mode of physisorbed water, surface hydroxyl groups and/or hydroxyl groups of by-product and the band at 1630 cm^{-1} is associated with O-H deformation mode. The weak band at about 2980 cm^{-1} is due to stretching vibration ν(CH) and the band at 1480 cm^{-1} is due to deformation vibration $\delta(CH_2)$. The band located around 1360 cm^{-1} can be attributed to the deformation vibration modes $\delta(OH)+\delta(CH_2)$ [24]. The relatively weak bands appearing at 1150 and 1070 cm^{-1} were tentatively assigned to the deformation vibration $\delta(CH_2)$ and antisymmetric stretching ν(C-O) [25] of alcohols. As mentioned above, several authors have reported the presence of carbonyl intermediates such as CH_3CHO, CH_3COCH_3 or $CH_3COC_2H_5$ [24,26,27]. In this work, the absence of the absorption band at 1700cm^{-1} allows to reject the presence of carbonyl derivatives as intermediates.

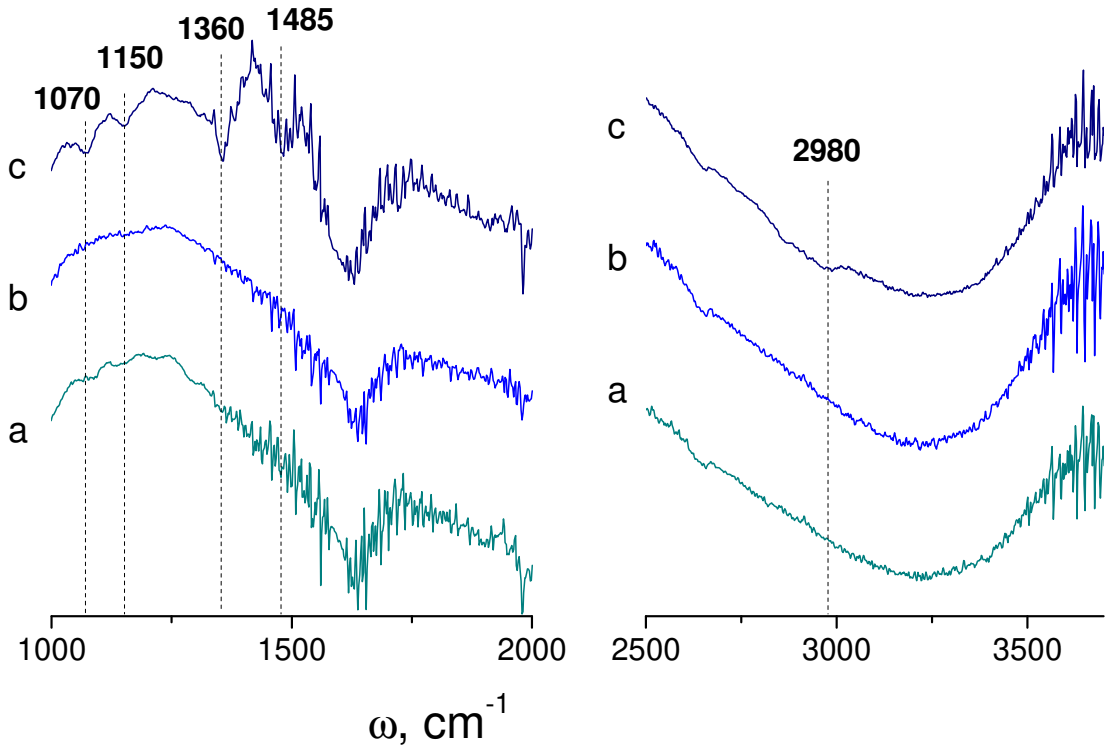

Figure 4. FTIR spectra of Fe(III)-TiO_2 photocatalyst (a) freshly prepared, (b) freshly prepared after being exposed to gaseous ethylene flow in dark for 3 hours and(c) after UVA illumination in presence of pollutant for 3 hours.

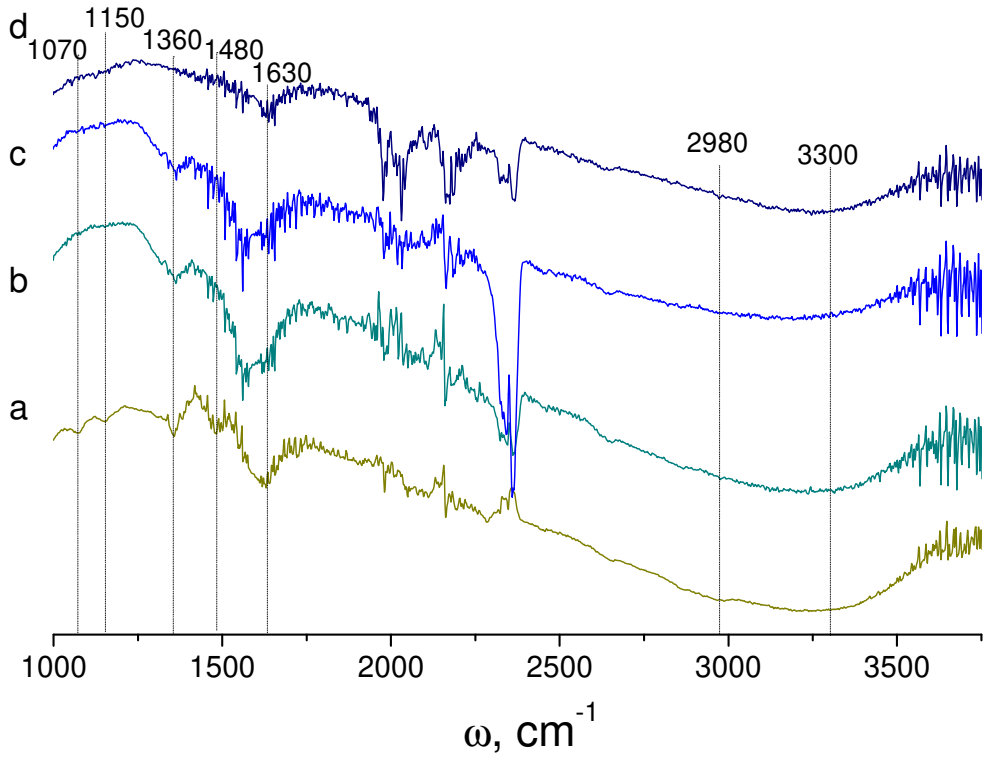

Figure 5. FTIR spectra of Fe(III)-TiO_2 photocatalyst: freshly prepared (a) and used after secondary thermal treatment for 1 hour at 100°C (b), 200 °C (c) and 300°C (d).

Several studies have been reported in the past on organic photopolymerization in presence of semiconducting solids. Popovićet al. [28] have observed polymerization of methacrylic acid on CdS, CdS/HgS and CdS/TiO_2 triggered by free holes photogenerated in valence band. Damm et al. [29] have compared UV photopolymerization of methyl tri-acrylate with P25-TiO_2 and anatase TiO_2 prepared by spray-hydrolysis. Strandwitz et al. [30] have examined the polymerization of pyrrole impregnated into mesoporous TiO_2 with the goal to obtain organic-inorganic hybrids. Li et al. [31] have analyzed photopolymerization of diacetylene in the presence of TiO_2 thin films. Ni et al. [32] and Dong and Ni [33] have performed the UVA assisted polymerization of methyl methacrylate in the presence of anatase TiO_2 and P25 TiO_2 particles dispersed in the aqueous monomer solutions. As these studies show, intermediates with high-molecular weight can be formed in photocatalytic experiments. The formation of high molar weight intermediates, as non-volatile polymeric hydrocarbons, apparently took place under UVA illumination of ethylene as in our experiments.

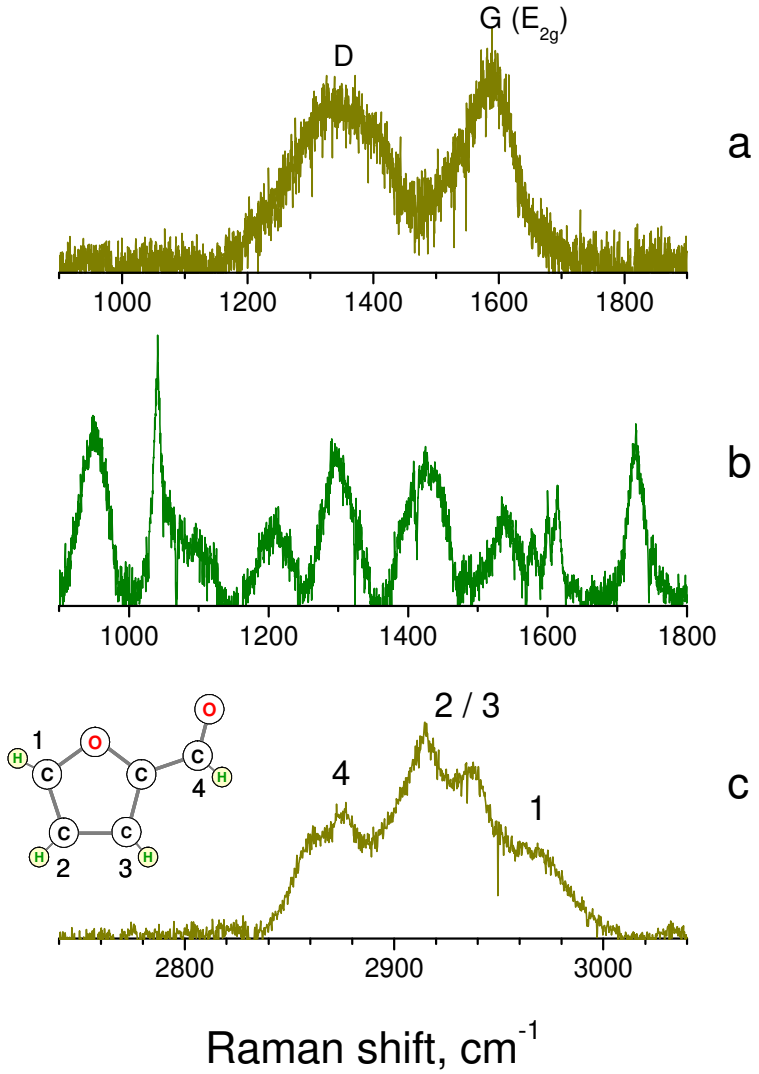

209

210 **Figure 6.** Raman spectra of the black (a) and white (b,c) solid products collected after the
211 photocatalytic process followed by the photocatalyst heating at 400 °C.

212 The direct analysis of the non-volatile reaction product was complicated by its small surface mass
213 density. In order to collect this product from the large photocatalyst surface, the heat treatment at
214 temperature ~400 °C under dry air flow was used. As a result, two kinds of compact solid products
215 were collected in the reactor output area: black particles and white semi-transparent filaments, which
216 masses ~0.1-1 mg were sufficient for the Raman analysis. Raman spectra of these products are shown
217 in Fig. 6. The black product (Fig. 6a) was identified with glassy carbon, which Raman spectrum shows
218 two characteristic resolved disorder-induced D and first-order allowed G (E_{2g}) bands [34]. The Raman
219 spectrum of the white product in Fig. 6b shows a complex structure containing multiple vibrational

bands; its assignment is less straightforward. Our analysis of available Raman spectra of ethylene and its oxidized and polymerized derivatives brought us to a conclusion about the formation of furan derivatives in the photocatalytic process [35]. In particular, the six observed bands between 900 and 1600 cm^{-1} shown in Fig. 6b fit the calculated Raman spectra of oligomers composed of 6 and 8 furan molecules [36]. Moreover, the band at 1730 cm^{-1} identified with the C=O vibration can be observed in polyfurane [37] and indicates the presence of the oxidized derivatives, the best candidate of which is furfural [35]. Because of this, we tentatively assign the deposited product to the furan and/or furfural oligomers (Ol_N). More evidence to the polyfurfural assignment can provide Raman analysis of the C-H vibration mode in the frequency range of ~3000 cm^{-1} presented in Fig. 6c. The observed spectral band has partially resolved structure, which belongs to CH groups of the molecule in different geometric positions. Given the structure of the furfural molecule shown in inset of Fig. 6c and tendencies of the frequency evolution [35], the subbands at 2875 cm^{-1}, 2915 cm^{-1}, 2937 cm^{-1} and 2970 cm^{-1} can be respectively assigned to the aldehyde CH stretching (4), antisymmetric and symmetricβ-CH stretching (2 / 3) and α-CH symmetricstretching (1) modes. Somewhat lower frequencies of the bands compared to those of the single furfural molecule can be attributed to a partial polymerization leading to the formation of furfural oligomers.

As observed in our experiments, the deposited solid products can be removed from the photocatalyst surface by a heat treatment at temperatures ~300 °C, as show the experimental results of Fig. 2 and Fig. 3. The photocatalyst regeneration could be explained by the oligomers desorption and/or thermal decomposition. In the same time, polyfuran is known to resist temperatures up to 400 °C [37,38], which may explain the successful collection of a small part of this product. Apart of these bands, we observed several narrow peaks at 1041, 1580, 1600 and 1614 cm^{-1} which may be related to C-C vibrations of minor carbonaceous species.

According to the above assignment, the photocatalytic oxidation of ethylene results in the formation of short polymeric chains of furan and furfural molecules on the photocatalyst surface. An increase of temperature results in the desorption of larger oligomers and thermal decomposition of smaller ones. The glassy carbon is formed as results of the thermal decomposition. In contrast, the larger polyfurans and polyfurfurals are stable and survive after the thermal desorption. Although we

248 were not optimised the desorption temperature permitting analysis of a full scope of non-damaged
249 surface products, the collected oligomers Ol_N (N=6÷8) evidences their formation at the photocatalyst
250 surface as one of major non-volatile products. Since the small Fe(III) doping 0.005 mol% does not
251 provide any significant modification of the titania band gap energy, surface area, etc. and only
252 improves the electron-hole separation efficiency [19], we expect the discussed mechanism of the
253 ethylene decomposition is the general feature of TiO_2-based photocatalysts.
254
255 3.2 Modeling
256 In this chapter, a kinetic model is proposed in order to suppose partial polymerisation of ethylene
257 and formation of oligomers, which do not desorb from the photocatalyst surface. The physical
258 significations of all introduced parameters were summarized in table 2:
259 Table 2: The physical signification of all introduced parameters

Symbol	Physical signification
E_g/E_{ads}	Gaseous/adsorbed ethylene
pE	Polymeric products
p	Gaseous reaction products (CO_2)
k	Reaction rate constant
n_0	Density per unitary volume of the active TiO_2 surface sites available for adsorption
n	Density per unitary volume of the active TiO_2 surface sites available for ethylene adsorption
m	Density per unitary volume of the active TiO_2 surface sites available for polymeric side products adsorption
y	Ratio between m et n_0
v	Pollutant flow rate through the reactor bed
L	Reactor length (30 cm)
E_a	activation energy

260
261 This process can be triggered by the photogenerated hole transfer to C=C double bonds. Both
262 adsorbed monomers and oligomers contribute to this process. The relevant reactions are:

263 $$E_g \xleftrightarrow{k_{eq}} E_{ads} \quad (1)$$

$$E_{ads} + E_g + h\nu \xrightarrow{k_1'} pE$$
264 $$pE + E_g + h\nu \xrightarrow{k_1''} pE \quad (2)$$
$$E_{ads} + h\nu \xrightarrow{k_2} p$$

$$pE + hv \xrightarrow{k_3} p \quad (3)$$

Where E_g/E_{ads}, pE and p stand for gaseous/adsorbed ethylene, adsorbed polymeric products and gaseous reaction products (CO_2), which are correspondingly defined as N/n, m and p in the following equations. The reaction order is 1. It is supposed that the adsorption/desorption process (1) is in equilibrium while photodecomposition reactions (2) and (3) are not.

The ethylene is known to be weakly adsorbed at the TiO_2 surface (E_a~3 kCal/mol or ~5kT at room temperature), while the heavy ethylene oligomers are totally adsorbed. Therefore, $n_0 >> n$ (here n_0 represents the density per unitary volume of the active TiO_2 surface sites available for adsorption). However, m slowly increases until $m_{t\to\infty} = n_0$. From (1) it can be obtained:

$$n = (n_0 - m)\frac{k_{eq}N}{1 + k_{eq}N} \quad (4)$$

The kinetic equation describing (2)-(3) are:

$$\frac{dm}{dt} = k_1^{'}nN + k_1^{''}(1 - m/n_0)mN - k_3 m \quad (5)$$

$$\frac{dp}{dt} = k_2 n + k_3 m \quad (6)$$

The second term of above Eq. (5) is completed by a factor ($1-m/n_0$), which takes into account the catalyst surface coverage by polymeric products. The equations (4)-(5) can be reduced to

$$\frac{dm}{dt} = k_1^{'}n_0\gamma N + (k_1^{''}N - k_1^{'}\gamma N - k_3)m - k_1^{''}N\frac{m^2}{n_0} \quad (7)$$

where $\gamma = \frac{k_{eq}N}{1 + k_{eq}N}$.

Eq. (7) is solved in approximation of a small coverage of TiO_2 by both monomers and oligomers: $n_0 >> n, m$ (we remark that this corresponds to $\gamma << 1$). For the sake of simplicity, it is supposed that the associations "monomer-monomer" and "polymer-monomer" propagate with the same constants $k_1^{'} = k_1^{''} \equiv k_1$. Moreover in order to explain the long-lasted accumulation of new species, it is assumed

that the polymerisation reaction dominate over the decomposition products formation: $k_1 N >> k_3$. Then Eq. (7) can be reduced to:

$$\frac{dy}{dt} = k_1 N\left(\gamma + y - y^2\right) = k_1 N(y - y_1)(y - y_2) \tag{8}$$

where $y = m / n_0$ ($y \in [0,1)$) and $y_{1,2} = (1 \pm \sqrt{1 + 4\gamma}) / 2$. Because $\gamma << 1$, Eq. (8) can be rewritten as:

$$\frac{dy}{dt} = k_1 N(y - 1)(y + \gamma) \tag{9}$$

The solution of Eq. (9) is

$$m = n_0 \frac{1 - e^{-k_1 N t}}{1 + e^{-k_1 N t} / \gamma} \tag{9}$$

In order to obtain the output ethylene concentration, it should consider the pollutants propagation through the reactor bed. Then the reduction of N(z) is related to the surface sites liberation due to the decomposition of both ethylene molecules and polymerised chains and it is relate to the rate of the products exit:

$$\frac{dN}{dz} = -\left(\frac{1}{2}\frac{dp}{dt} + \frac{dm}{dt}\right)\frac{dt}{dz} \approx -\frac{1}{2v}\frac{dp}{dt} \tag{10}$$

where v is the pollutant flow rate through the reactor bed. It is assumed here that dm/dt is a slow function of time (characteristic time of the polymerisation is ~1 hour) while dp/dt is a quick function of time (characteristic residence time of gas molecules in the reactor bed is ~1 s). One can rewrite Eq. (10) as

$$\frac{dN}{dz} = -\frac{1}{2v}\left(k_2 n + k_3 m\right) = -\frac{n_0}{2v}\left[k_2\gamma + (k_3 - k_2\gamma)m\right] \tag{11}$$

or

$$\frac{dN}{dz} = -\alpha N + (\beta - \alpha N)\frac{1 - e^{-k_1 N t}}{1 + e^{-k_1 N t} / k_{eq} N} \tag{12}$$

where $\alpha = k_2 k_{eq} n_0 / 2v$ and $\beta = k_3 n_0 / 2v$ ($0 \le z \le L$ =30 cm). Eq. (12) is numerically solved in order to fit the experimental data with four free parameters α, β, k_1 and k_{eq}. The best fit with α=0.023, β=0.9, k_1=0.00055 and k_{eq}=0.012 is shown in Fig. 7 by dotted line.

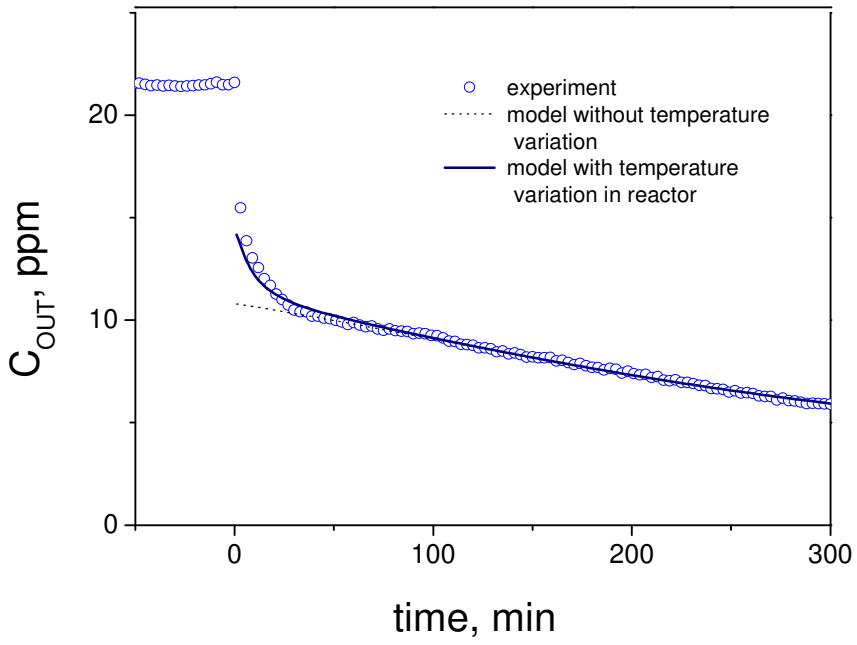

308

309 **Figure 7.** Ethylene concentration at the photocatalytic reactor exit versus time (experiment and
310 modelling).

311 The agreement between the model and experiment is good except of the early reaction times.
312 Since the lamp attains a stationary luminosity within three minutes, the transient period t≤50 min is
313 attributed to the activation of photocatalytic reactions. Indeed as the measurements show (Fig. 2), the
314 reactor temperature increases at this stage.

315 Since the ethylene polymerisation progresses slowly, it is assumed that the ethylene
316 decomposition is affected by the temperature increase: $k_2 = k_{20} \cdot \exp(E_a / kT)$. The complete least
317 squared fit of the experimental kinetics with Eq. (12) including $k_2(T)$ with E_a=19±2kJ/mol is shown
318 in Fig. 7 by solid line.

319 The validity of the model assumptions was check in the following section. From the fit, the
320 equilibrium constant is small indeed. The fit also results in the reaction constants ratio
321 $k_2 / k_3 = \alpha / \beta k_{eq} \approx 2.1$, which signifies that the photocatalytic decomposition of ethylene is easier
322 than that of oligomers. One can see that the assumption $k_1 N \ll k_3$ holds, because $k_1 N = 0.0121$ and
323 $k_3 = 0.9 \cdot 2 \cdot v / n_0 = 580 / n_0 \approx 7 \cdot 10^{-4}$ (gas speed: v=30cm/5.7s=5.3 cm/s=318 cm/min,

$n_0 = m_{TiO_2} S_{BET} / S_{molec} \approx 10^{-2} \cdot 200/10^{-19} = 8 \cdot 10^5$ ppm if $m_{TiO_2} = 10^{-2}$ g is used on 30 cm long reactor bed and $S_{molec} = 0.1$ nm^2). The photocatalytic process is generally found not very sensitive to temperature with activation energies in the range between 5 and 16 kJ/mol [39]. The apparent activation energy of ethylene degradation over TiO_2 of 13.9-16.0 kJ/mol has been reported by Yamazaki et al.[39]. Our value of E_a fits the upper limit of the earlier reported values. It is concluded that the proposed theoretical model is quite satisfactory.

The proposed theoretical model successfully explained the experiment, suggesting polymerisation of ethylene initiated by UVA photons at the photocatalyst surface. In agreement with our previous studies of light-induced processes at the organic-TiO_2 interface, the photogenerated hole can efficiently escape the inorganic solids into surrounding organics[40,41]. Its localisation on a C=C double bond of ethylene molecule will provoke its opening that initiates polymerisation process.

IV. Conclusion

In this work the decomposition kinetics of gaseous ethylene onto the optimized Fe(III)-TiO_2 anatase photocatalyst with Fe/Ti ratio of 0.005 mol% was studied in a continuous-flow fixed-bed reactor. Based on FTIR, Raman and thermal post-treatment analyses, it was concluded about the formation of a major non-volatile intermediate reaction product in course of the ethylene decomposition, assigned to the oxidized polymeric hydrocarbons: furan and furfural oligomers Ol_N with N=6÷8. The analysis of the photocatalytic process kinetics showed that this product covers the photocatalyst surface and delays the stationary reaction kinetics.

A theoretical model is proposed explaining the process kinetics. The overall photo-assisted process therefore includes two main stages: (i) on the first one, the high-molecular mass product is synthetized enhancing contact with the photocatalyst surface (in contrast to weakly adsorbing ethylene molecules) and (ii) on the second one, the heterogeneous decomposition of the non-volatile species takes place. A weaker rate constant of the oligomers decomposition (as compared with ethylene gas) is compensated by their much stronger adsorption, which enhances the overall reactor yield. The oligomers decomposition can be thermally activated with E_a=19±2 kJ/mol.

Acknowledgments

This work is supported by French C'Nano (IdF) network.

356 References

357 [1] U.I. Gaya, A.H. Abdullah, J. Photochem. Photobiol. C Photochem. Rev. 9 (2008) 1–12.

358 [2] H. Zhang, W. Wang, H. Zhao, L. Zhao, L.-Y. Gan, L.-H. Guo, ACS Catal. 8 (2018) 9399–
359 9407.

360 [3] J. Ma, H. He, F. Liu, Appl. Catal. B Environ. 179 (2015) 21–28.

361 [4] S. Sun, J. Ding, J. Bao, C. Gao, Z. Qi, X. Yang, B. He, C. Li, Appl. Surf. Sci. 258 (2012)
362 5031–5037.

363 [5] Z. Jia, M. Ben Amar, O. Brinza, A. Astafiev, V. Nadtochenko, A.B. Evlyukhin, B.N.
364 Chichkov, X. Duten, A. Kanaev, J. Phys. Chem. C 116 (2012) 17239–17247.

365 [6] Z. Jia, M. Ben Amar, D. Yang, O. Brinza, A. Kanaev, X. Duten, A. Vega-González, Chem.
366 Eng. J. 347 (2018) 913–922.

367 [7] X. Chen, R. Li, X. Pan, X. Huang, Z. Yi, Chem. Eng. J. 320 (2017) 644–652.

368 [8] X. Liang, P. Wang, M. Li, Q. Zhang, Z. Wang, Y. Dai, X. Zhang, Y. Liu, M.H. Whangbo, B.
369 Huang, Appl. Catal. B Environ. 220 (2018) 356–361.

370 [9] N. Pathak, O.J. Caleb, M. Geyer, W.B. Herppich, C. Rauh, P. V. Mahajan, Food Bioprocess
371 Technol. 10 (2017) 982–1001.

372 [10] D.-R. Park, J. Zhang, K. Ikeue, H. Yamashita, M. Anpo, J. Catal. 185 (1999) 114–119.

373 [11] S. Yamazaki, S. Tanaka, H. Tsukamoto, J. Photochem. Photobiol. A Chem. 121 (1999) 55–61.

374 [12] K. Bhattacharyya, S. Varma, K. Kishore, N.M. Gupta, Res. Chem. Intermed. 32 (2006) 17–30.

375 [13] W.-D. Wang, A. Bakac, J.H. Espenson, Inorg. Chem. 34 (1995) 6034–6039.

376 [14] H. Einaga, Y. Teraoka, Res. Chem. Intermed. 34 (2008) 617–628.

377 [15] G.Y. Popova, T. V. Andrushkevich, Y.A. Chesalov, E.S. Stoyanov, Kinet. Catal. 41 (2000)
378 805–811.

379 [16] B. Hauchecorne, T. Tytgat, S.W. Verbruggen, D. Hauchecorne, D. Terrens, M. Smits, K.
380 Vinken, S. Lenaerts, Appl. Catal. B Environ. 105 (2011) 111–116.

381 [17] M. Anpo, K. Chiba, M. Tomonari, S. Coluccia, M. Che, M.A. Fox, Bull. Chem. Soc. Jpn. 64
382 (1991) 543–551.

383 [18] S. Tieng, R. Azouani, K. Chhor, A. Kanaev, J. Phys. Chem. C 115 (2011) 5244–5250.

[19] S. Tieng, A. Kanaev, K. Chhor, Appl. Catal. A Gen. 399 (2011) 191–197.

[20] Y. Ichihashi, Y. Matsumura, Res. Chem. Intermed. 29 (2003) 891–896.

[21] V. Keller, P. Bernhardt, F. Garin, J. Catal. 215 (2003) 129–138.

[22] G. Pecchi, P. Reyes, T. López, R. Gómez, A. Moreno, J.L.G. Fierro, A. Martínez-Arias, J. Sol-Gel Sci. Technol. 27 (2003) 205–214.

[23] M. Benmami, K. Chhor, a V Kanaev, J. Phys. Chem. B 109 (2005) 19766–71.

[24] B. Hauchecorne, D. Terrens, S. Verbruggen, J.A. Martens, H. Van Langenhove, K. Demeestere, S. Lenaerts, Appl. Catal. B Environ. 106 (2011) 630–638.

[25] W. Sawodny, K. Niedenzu, J.W. Dawson, Spectrochim. Acta Part A Mol. Spectrosc. 23 (1967) 799–806.

[26] G.Y. Popova, T. V. Andrushkevich, Y.A. Chesalov, E.S. Stoyanov, Kinet. Catal. 41 (2000) 805–811.

[27] M. Anpo, K. Chiba, M. Tomonari, S. Coluccia, M. Che, M.A. Fox, Bull. Chem. Soc. Jpn. 64 (1991) 543–551.

[28] I.G. Popović, L. Katsikas, H. Weller, Polym. Bull. 32 (1994) 597–603.

[29] C. Damm, D. Völtzke, H.-P. Abicht, G. Israel, J. Photochem. Photobiol. A Chem. 174 (2005) 171–179.

[30] N.C. Strandwitz, Y. Nonoguchi, S.W. Boettcher, G.D. Stucky, Langmuir 26 (2010) 5319–5322.

[31] L. Li, Y. Wang, F. Yan, L.A. Samuelson, J. Kumar, J. Macromol. Sci. Part A 47 (2010) 1161–1166.

[32] X. Ni, J. Ye, C. Dong, J. Photochem. Photobiol. A Chem. 181 (2006) 19–27.

[33] C. Dong, X. Ni, J. Macromol. Sci. Part A 41 (2004) 547–563.

[34] Y. Wang, D.C. Alsmeyer, R.L. McCreery, Chem. Mater. 2 (1990) 557–563.

[35] T. Kim, R.S. Assary, L.A. Curtiss, C.L. Marshall, P.C. Stair, J. Raman Spectrosc. 42 (2011) 2069–2076.

[36] C. Liu, J. Zhang, G. Shi, Y. Zhao, J. Phys. Chem. B 108 (2004) 2195–2199.

[37] X.G. Li, Y. Kang, M.R. Huang, J. Comb. Chem. 8 (2006) 670–678.

[38] G. Tourillon, F. Garnier, J. Electroanal. Chem. Interfacial Electrochem. 135 (1982) 173–178.

[39] A. Mills, S. Le Hunte, J. Photochem. Photobiol. A Chem. 108 (1997) 1–35.

[40] A. Uklein, P. Gorbovyi, M. Traore, L. Museur, A. Kanaev, Opt. Mater. Express 3 (2013) 533.

[41] A.I. Kuznetsov, O. Kameneva, N. Bityurin, L. Rozes, C. Sanchez, A. Kanaev, Phys. Chem. Chem. Phys. 11 (2009) 1248.

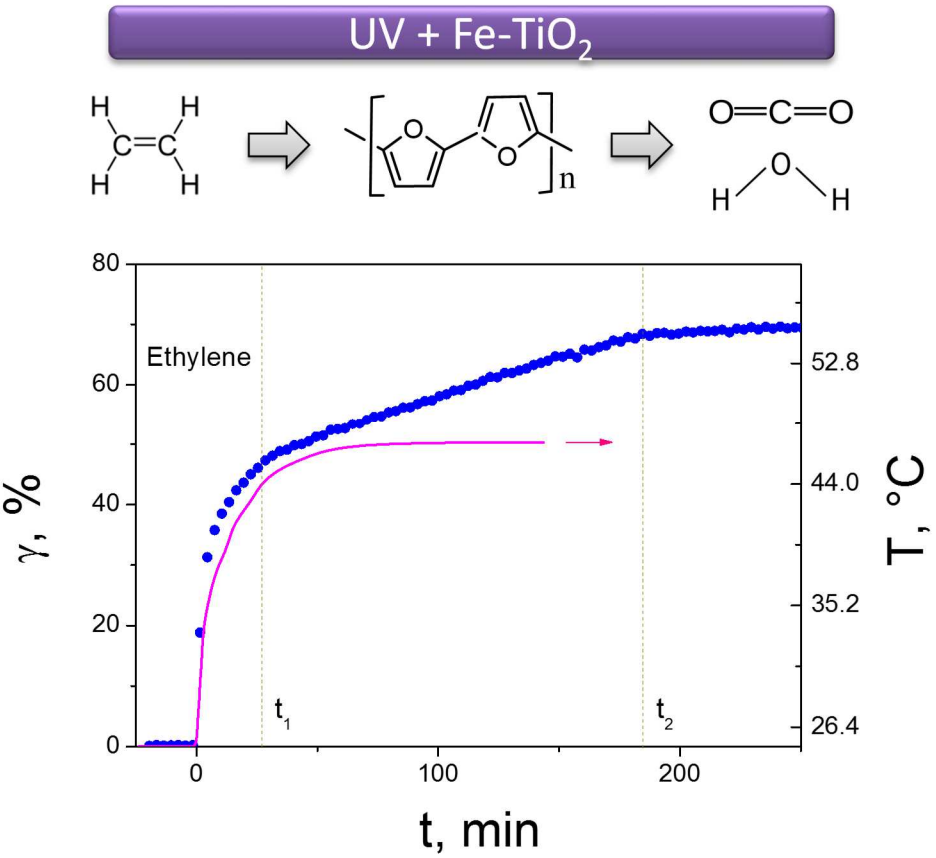
UV + Fe-TiO2
H
C=C
H
H
H
O
n
O=C=O
O
H
H
Ethylene
t1
t2
80
60
40
20
0
0
100
200
t, min
γ, %
52.8
44.0
35.2
26.4
T, °C